Title
Kinetics of Co-Mingled 99Tc and Cr Removal during Mineral Transformation of Ferrous Hydroxide

Journal
ACS Earth and Space Chemistry, 4(2)

ISSN
2472-3452

Authors
Saslow, Sarah A
Pearce, Carolyn I
Bowden, Mark E
et al.

Publication Date
2020-02-20

DOI
10.1021/acsearthspacechem.9b00277

Peer reviewed

Kinetics of Co-Mingled ^{99}Tc and Cr Removal During Mineral Transformation of Ferrous Hydroxide

Sarah A. Saslow[1], Carolyn I. Pearce[1], Mark E. Bowden[2], Wayne W. Lukens[3], Dong-Sang Kim[1], Albert A. Kruger [4], and Wooyong Um[1,5,6,*],

[1]*Pacific Northwest National Laboratory, Richland, WA, 99354, USA*

[2]*Environmental Molecular Sciences Laboratory, Pacific Northwest National Laboratory, Richland, WA, 99354, USA*

[3]*Lawrence Berkeley National Laboratory, 1 Cyclotron Rd, Berkeley, CA, 94720 USA*

[4]*United States Department of Energy, Office of River Protection, P.O. Box 450, Richland, WA 99352, United States*

[5]*Division of Advanced Nuclear Engineering (DANE)/Division of Environmental Science and Engineering (DESE), Pohang University of Science and Technology (POSTECH), Pohang, 790-784, Republic of Korea*

[6]*Nuclear Environmental Technology Institute (NETI), Pohang University of Science and Technology (POSTECH), Pohang, Gyeongbuk 790-784, Republic of Korea*

*Corresponding author: Wooyong Um, Pacific Northwest National Laboratory, 902 Battelle Blvd., PO Box 999, P7-54, Richland, WA 99352, USA. Telephone: (509)-371-7175. Fax: (509)-371-7344. Now at Pohang University of Science and Technology (POSTECH); Email address: wooyongum@postech.ac.kr

25
26

Abstract

Four simulated waste streams relevant to the vitrification of Hanford nuclear waste were studied to the evaluate the removal kinetics of technetium-99 (Tc) and co-mingled Cr(VI) during treatment with solid ferrous hydroxide ($Fe(OH)_2(s)$). Simulants were: (i) 1 M NaOH (control system), (ii) 1M NaOH solution with 1570 ppm Cr(VI), (iii) secondary off-gas (OG) waste stream simulant, and (iv) 5M Na LAW (low activity waste). Simulants treated with $Fe(OH)_2(s)$ were reacted for 24 hours and sub-sampled periodically to monitor Tc and Cr(VI) removal. Solution sample analysis during the reaction was coupled with solid phase characterization, e.g. X-ray absorption spectroscopy (XAS) and X-ray diffraction (XRD), to establish influence of the solid phase product on Tc and Cr(VI) removal rates. Based on these results, the majority of Tc and Cr(VI) removal occurs within the first five minutes of simulant contact with $Fe(OH)_2(s)$. However, the order in which Tc and Cr(VI) are completely removed from each simulant depends on the simulant chemistry, the preferred reduction pathway, and the nature of the solid phase product, e.g. magnetite (Fe_3O_4) versus goethite (α-FeOOH). Low pH and low Cr(VI) concentrations favor rapid Tc removal, with XRD and XAS confirming that Fe_3O_4 readily incorporates reduced Tc(IV) into its structure. High pH, high Cr(VI) concentrations, and the presence of other co-mingled constituents, favor heterogenous Tc removal early in the reaction (<1 hours). At reactions times >1 hour, Tc removal slows as homogenous reduction and

49 removal of Cr(VI) starts to dominate, concurrent with an increase in the
50 formation of FeOOH as the solid phase reaction product.

1. Introduction

The US Department of Energy Hanford Site is tasked with the vitrification of ~54 million gallons of liquid nuclear waste that is currently stored onsite in underground tanks.[1,2] One of the challenges associated with this approach is the generation of secondary waste streams to collect hazardous radionuclides that are volatilized under vitrification operating temperatures (>1000 °C). Technetium-99 (Tc) is a radioactive fission product that persists in the low activity waste streams at Hanford and is susceptible to volatilization. Due to its long half-life ($2.1x10^5$ years), high fission yield (~6%), and environmental mobility as Tc(VII) species in oxidizing environments,[3-5] Tc has been the focus of intense research to support site operations and cleanup. Specifically, the development of sequestration technologies or additives that can minimize volatilization, or be used to separately treat Tc in secondary waste streams, are currently being tested.[1,6-12] However, treatment of ~~Tc~~ Tc-containing waste streams, both before and after vitrification, has two major challenges: (i) reduction of Tc(VII) to less mobile and less volatile Tc(IV) in the presence of co-mingled redox-sensitive constituents, e.g. Cr(VI), nitrate (NO_3^-); and (ii) Tc stabilization in a phase that inhibits reoxidation and release into secondary waste streams or the environment.

To overcome these challenges, the use of solid ferrous hydroxide, ~~(~~$Fe(OH)_2(s)$,~~)~~ to reduce Tc(VII) in the presence of redox-competitors, and immobilize Tc(IV) in Fe (oxyhydr)oxide minerals formed during $Fe(OH)_2(s)$

oxidation, has been studied.[1,6,10-12] In these studies, $Fe(OH)_2(s)$ was successful at reducing and sequestering Tc to varying levels even in the presence of co-mingled constituents. The research shows that the extent of Tc reduction is highly dependent on the composition of the nuclear waste stream, e.g. secondary constituents, pH, E_h, and that incorporation of reduced Tc into a stable solid phase is dependent on the mineralogical composition of the reaction product. However, an investigation into the kinetic processes that drive Tc and co-mingled contaminant, e.g. Cr, removal by $Fe(OH)_2(s)$ and solid phase formation has not yet been undertaken for pertinent nuclear waste streams. Such studies are necessary for defining a representative treatment period to be accounted for in waste processing procedures, where treatments requiring a few minutes as opposed to days are less likely to inhibit waste treatment and throughput.

Although monitoring rate of removal by measuring total Tc and Cr concentrations in solution is not a direct measure of reduction, negligible sorption of the TcO_4^- or CrO_4^{2-} oxyanions is expected, as the $Fe(OH)_2$ mineral surface will be negatively charged under the alkaline conditions in this system.[13] Thus, constituent removal from solution via precipitation or incorporation into the mineral phase is expected to be concurrent with reduction. Tc(VII) and Cr(VI) reduction is expected to proceed via heterogeneous and/or homogeneous pathways, where heterogenous reduction is a surface mediated process, e.g. interactions with Fe(II) sorbed to an iron oxide surface and Fe(II)/Fe(III) electron transfer,[14-17] and

homogenous reduction occurs in solution, e.g. $Fe(II)_{aq}$. As reported in previous studies, the reduction of Tc(VII) to Tc(IV) often favors heterogeneous reduction where electron density is higher at mineral surfaces compared to Fe(II) in solution.[14-17] Furthermore, Fe(II) sorbed on the surface of iron oxides is a more effective heterogeneous pathway for Tc reduction than Fe(II) trapped within a crystal lattice, e.g. magnetite ($Fe(II)Fe(III)_2O_4$).[17] Thermodynamically, homogeneous reduction of Tc(VII) is also possible, but kinetically hindered as a three-step single-electron reduction process.[14,15,18-20] Comparatively, Cr(VI) homogeneous reduction to Cr(III) occurs nearly instantaneously in the presence of $Fe(II)_{aq}$, due to a more oxidizing Cr(VI)/Cr(III) redox couple (+1.34 V) compared to Tc(VII)/Tc(IV) (+0.748 V),[16] and the heterogeneous pathway is often slower.[18,21-23] The Fe(II) capacity for targeted Tc and Cr treatment, and the rate of reduction, are expected to be influenced by the presence of dissolved oxygen and redox-sensitive anions, e.g. NO_2^-, NO_3^-, SO_4^{2-}, and PO_4^-, for both heterogeneous and homogeneous reduction pathways.

Herein, four simulated waste streams relevant to the Hanford Site, and with varying Cr concentrations, pH, E_h, and other co-mingled constituents, were studied to evaluate trends in the kinetics driving reduction and removal of Tc and Cr, over a 24 hour period. These simulants were (i) 1 M NaOH solution (control system), (ii) 1M NaOH solution with 1570 ppm Cr(VI) to evaluate effect of Cr(VI) on Tc removal kinetics under high alkaline environments, (iii) off-gas (OG) simulant to mimic the secondary waste

stream containing volatilized Tc, and (iv) 5M Na LAW (low activity waste) simulant to evaluate waste treatment by $Fe(OH)_2(s)$ prior to vitrification. Simulant aliquots were treated with $Fe(OH)_2(s)$ and allowed to react for 24 hours at 75°C. Periodic sampling was used to monitor the removal of Tc and Cr from solution. Solution analyses to determine trends in Tc and Cr(VI) removal rates were coupled with solid phase characterization, e.g. X-ray absorption spectroscopy (XAS) and X-ray diffraction (XRD), to identify the solid phase reaction product. Experimental variables including pH, Cr(VI) concentration, and co-mingled redox sensitive anions, e.g. NO_3^-, are expected to influence the order in which contaminants are removed from solution, the Fe oxide/oxyhydroxide reaction product, and the Tc loading capacity of these stable solid phases. All variables and outcomes have implications for the treatment of nuclear waste streams and identifying the optimal implementation pathway within planned nuclear waste processing operations.

2. Experimental

$Fe(OH)_2(s)$ Synthesis. The synthesis procedure and product characterization for $Fe(OH)_2(s)$ may be found in previously published work.[6,11] Briefly, $Fe(OH)_2(s)$ was prepared and stored inside an anoxic chamber (Coy Laboratories) that was maintained using a gas mix of N_2 (98%) and H_2 (2%). Ferrous iron (Fe(II)) was sourced from 14 g of $FeCl_2 \cdot 4H_2O$ (>95%, Fisher Scientific) and dissolved in 400 g of N_2-purged double deionized water (DDI, Millipore 18 Ω). The dissolved Fe(II) was then precipitated as $Fe(OH)_2(s)$ by

adding 8.2 mL of 10 M NaOH (Fisher Scientific) to solution followed by hand mixing. The solid was reacted overnight and then separated from the supernatant using a sterile 0.45 µm Nalgene® filter. $Fe(OH)_2(s)$ was dried completely over the course of 24-48 hours. Within 24 hours before use, $Fe(OH)_2(s)$ was ground into a powder using a mortar and pestle and the desired mass pre-weighed into a 20 mL polybottle.

Simulant Preparation. Four simulated waste streams were used in this work: a 1 M NaOH solution, a 1 M NaOH solution containing ~1570 ppm Cr(VI), an average 5 M Na low activity waste (LAW) simulant with ~1100 ppm Cr(VI), and an off-gas (OG) simulant with ~90 ppm Cr(VI). The Cr(VI) concentration in the 1 M NaOH simulant matrix (95% NaOH pellets, Fisher Scientific) was adjusted using $Na_2Cr_2O_7 \cdot 2H_2O$ (≥99.5%, Allied Chemical). Previously published procedures for the OG and LAW simulants were also used in this work.[6,24,25] Each simulant, depending on the desired experimental conditions, was also spiked with 1 or 100 ppm Tc(VII) using a 10,000 mg/L Tc stock solution (NH_4TcO_4). The starting composition of each simulant was confirmed for each prepared sample by inductively coupled plasma – optical emission spectroscopy (ICP-OES), ICP-mass spectrometry (ICP-MS), and/or ion chromatography (IC). Measured pH and E_h values for select simulants and reacted supernatants were also determined. Simulant composition, pH, and E_h (standard hydrogen electrode corrected) results are reported in Table 1.

Table 1. Simulant Compositions

Constituent	1 M NaOH	1 M NaOH + Cr	LAW	OG
	ppm	*ppm*	*ppm*	*ppm*

Al	-	-	8410 ± 570	26 ± 1
Cr	-	1570 ± 80	1100 ± 50	90 ± 1
Pb	-	-	48 ± 6	-
P	-	-	910 ± 40	5 ± 1
K	-	-	1300 ± 110	121 ± 7
Na	22,900 ± 1800	23,200 ± 1700	119,000 ± 9000	2650 ± 60
S	-	-	2810 ± 230	810 ± 10
NH_4^+	-	-	-	1950**
F^-	-	-	<1000*	1450**
Cl^-	-	-	<2500*	950**
NO_2^-	-	-	26,800*	10**
Br^-	-	-	<5000*	-
NO_3^-	-	-	102,000*	4770**
SO_4^{2-}	-	-	10,100*	2340**
PO_4^{3-}	-	-	<7500*	17**
pH	13.3	13.5	13.5	5.6
E_h (Initial), mV	124	90 ± 32	79 ± 1	408 ± 10
E_h (Final), mV	81 ± 7	68 ± 8	26	284

* Values from Saslow et al. 2018[6]

** Calculated values based on simulant recipe, same recipe used in Wang et al. 2019.[10]

Kinetics of Tc(VII) and Cr(VI) Removal by $Fe(OH)_2$(s). For all kinetic experiments, 0.60 – 0.75 g of $Fe(OH)_2$(s) was removed from the anoxic chamber and immediately added to 12 – 15 mL of simulant to achieve a $Fe(OH)_2$(s) mass to simulant volume ratio of 50 g/L. Based on previous work,[6,11] 50 g/L is the minimum ratio required to completely or partially remove 1 ppm of Tc in the presence of 1570 – 1080 ppm Cr(VI). Once combined, samples reacted for 24 hours (± 1 hour) in air and in an oven set to 75°C. During the reaction period, supernatant sub-samples of 0.2 – 0.5 mL were taken with a pipette approximately 5, 10, 30, 60, and 360 minutes after starting the reaction to monitor Tc and Cr removal. Sub-sampling required the sample to be removed from the oven for ~1 minute. After 24 hours, the

177 oven was turned off and the samples allowed to cool inside the oven for at
178 least two hours before the solid material was filtered (0.45 µm Nalgene®
179 filter), rinsed with ~50 mL of DDI, and air-dried for at least 24 hours. Aliquots
180 of the supernatant and DDI rinse were collected separately for total Cr
181 analysis by ICP-OES and total Tc analysis by ICP-MS. Total Tc, Cr, and Fe
182 concentrations were used to monitor constituents throughout the 24-hour
183 reaction period and calculate constituent removal rates.

184 **X-ray Diffraction (XRD).** Select dry solids were prepared for XRD
185 analysis by homogenizing the dry sample into a powder using a mortar and
186 pestle. Powder sub-samples were then weighed and spiked with ~10 weight
187 % internal standard (TiO_2, Sigma Aldrich) and re-homogenized before
188 analysis. XRD patterns were collected using a Rigaku Miniflex II XRD unit
189 equipped with a Cu Kα radiation (λ=1.5418 Å at 30-40 kV and 15 mA)
190 source. Samples were scanned at minimum between 3 and 90 degrees 2θ at
191 20 seconds per step and a step size of 0.05 degrees. Rietveld refinements
192 were performed using Bruker TOPAS software (v5, Bruker AXS, Germany)
193 with crystal structures obtained from the Inorganic Crystal Structure
194 Database (Fachinformationszentrum Karlsruhe, Germany). Since the angular
195 resolution of the instrument is 0.005 degrees 2θ, differences of <0.01 Å for
196 diffraction angles greater than 10 degrees 2θ are resolved during
197 quantification.

198 **X-ray Absorption Near Edge Structure (XANES) and Extended X-ray**
199 **Absorption Fine Structure (EXAFS) Spectroscopy.** XANES and EXAFS

were used to determine the bulk oxidation state and/or local coordination environment, respectively, of Tc and Cr within collected solids exposed to 100 ppm Tc in the starting simulant. Samples were prepared by homogeneously packing a portion of damp solid (collected immediately after filtering) into a Teflon window with Kapton tape sealing one side. Once packed, a second piece of Kapton tape was used to enclose the sample and then the window thoroughly sealed on all sides with additional Kapton tape. Sample windows were individually heat sealed into a plastic and Mylar bag for a total of three layers of containment. Samples were shipped to the Stanford Synchrotron Radiation Laboratory (SSRL) while adhering to SSRL radiological sample shipment procedures.

Tc K edge (21044 eV) spectra were collected under ambient conditions on SSRL beamline 11-2 and Cr K edge (5989 eV) spectra were collected on SSRL beamline 4-1. For Tc, data were obtained from 250 eV below the edge to ~900 eV above the edge. Data from 20 eV below the edge to 30 eV above the edge was obtained with 0.5 eV spacing and data from $1.62 \leq k \leq 15.2$ in the EXAFS region were collected in 0.05 increments weighted by k^3. Pre-edge data were collected in increments of 10 eV. At the Cr K edge, XANES data were obtained from at least 200 eV below the edge to 600 eV above the edge. Data from 30 eV below the edge to 20 eV above the edge was obtained with 0.3 eV spacing. Data from $1.65 \leq k \leq 5.2$ in the XANES spectrum were collected at 0.05 increments weighted by k^3 and the remaining data points were collected in 1 eV increments also weighted by k^3.

Cr pre-edge data were also collected in increments of 10 eV. The monochromator was detuned 50% for Tc and 70% for Cr to reduce the harmonic content of the beam. Transmission data was obtained using N_2 (Cr) or Ar (Tc) filled ion chambers. Fluorescence data was obtained using a 100 element (11-2) or 32 element (4-1) Ge detector.

Data were dead time corrected and reduced from raw data to spectra using SixPack.[26] ATHENA software was used to normalize collected spectra and to perform a linear combination analysis (LCA) using standard spectra.[27] XANES spectra for Tc and Cr were energy calibrated using TcO_4^- adsorbed on Reillex-HPQ polymer resin or Cr foil as the energy reference, respectively. The sample XANES spectra were allowed to vary in energy during LCA fitting. Shell-by-shell fitting of Tc K-edge EXAFS spectra was performed using ARTEMIS software.[27]

3. Results and Discussion

Early Tc and Cr Removal (0 – 0.08 hours). Trends in Tc and Cr removal from simulants over the course of 24 hours are shown in Figure 1. Immediately apparent is the rapid removal of 8 – 96 % of both constituents within the first 0.08 hours (5 minutes) of the reaction. In the OG and LAW simulants, the difference in Tc and Cr removal percentages are ≤ 13% (some within experimental error), suggesting that changes to the aqueous environment impact removal of Tc and Cr similarly. However, in the 1 M NaOH + Cr system, Tc removal is 15 – 43 % less than Cr removal, suggesting that these high pH, high Cr conditions promote homogeneous reduction over

heterogeneous processes in the early stages of reaction, and facilitate more Cr removal compared to Tc.

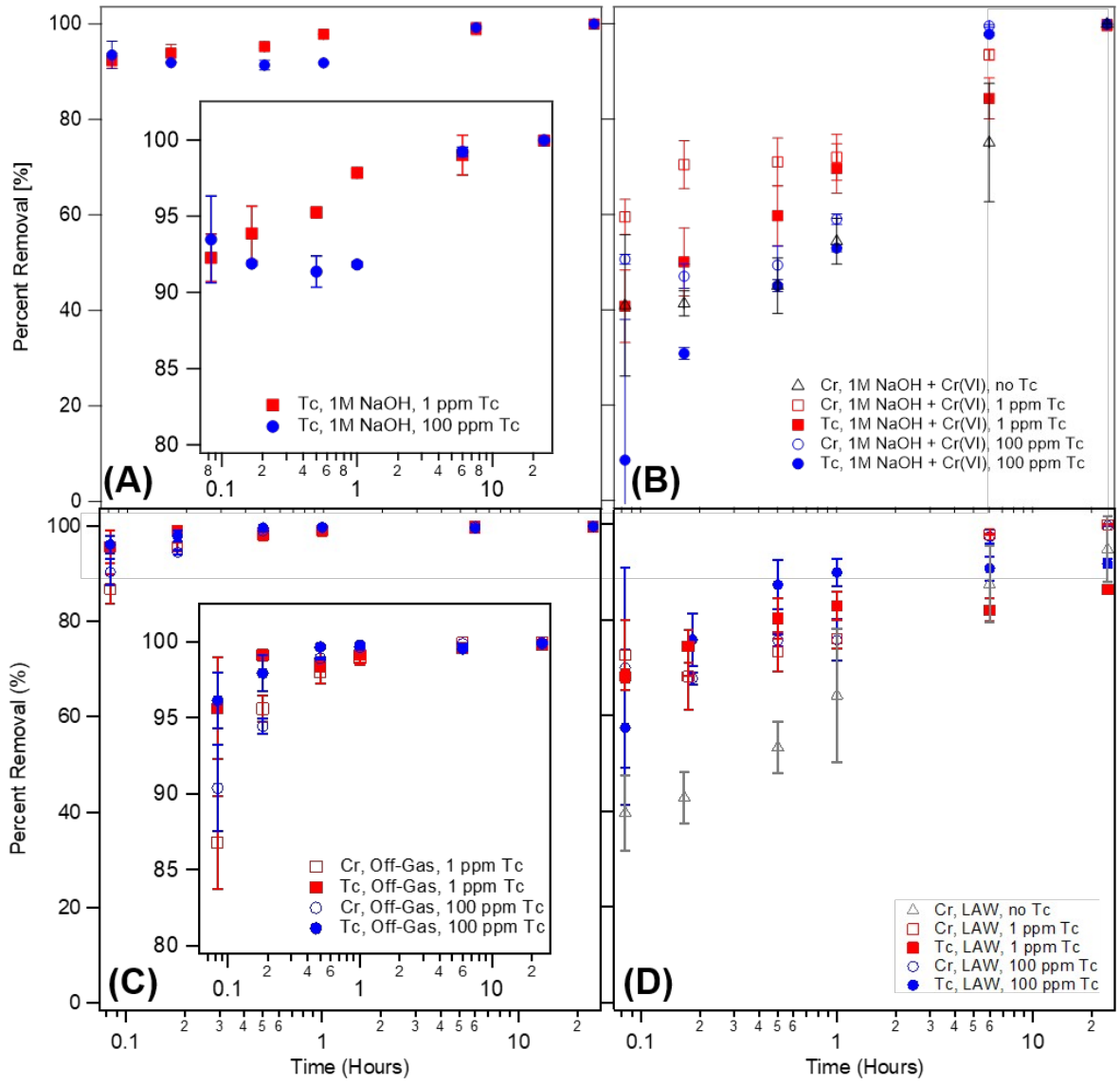

Figure 1. Removal of Tc and/or Cr as a function of time in (A) 1M NaOH, (B) 1M NaOH + Cr, (C) OG Simulant, and (D) LAW Simulant. Error bars indicate the standard deviation (1σ) of the average value determined from two to four replicate samples.

To quantify the effect of the simulant on rate of removal for metals with vastly different initial concentrations, initial rates were calculated as a fraction of the starting concentration, $([M]_0 - [M]_t)/[M]_0$ (where M = Tc or Cr, $[M]_0$ = concentration of metal at 0 hr, and $[M]_t$ = concentration of metal at 0.08 hr), versus time (0.08 hr) for each initial Tc concentration (0, 1, and/or 100 ppm) and simulant studied (Table S1 and). For Fe, the initial concentration in each simulant was non-detect; therefore, the presence of Fe in solution after 0.08 hr would suggest release of Fe from the solid as a result of $Fe(OH)_2(s)$ dissolution. In these cases, the mol fraction of Fe released Fe_t/Fe_0 (where Fe_0 = the total moles of Fe in $Fe(OH)_2(s)$ added at 0 hr, and Fe_t = moles of Fe in solution at 0.08 hr), versus time is used to calculate Fe release rate.

Table 2. Early (0 – 0.08 hrs) Removal and Release Rates for Tc, Cr, and Fe Constituents

Simulant	Initial [Tc], ppm	Early Removal Rate (% removed hr^{-1})		Early Release Rate (% released hr^{-1})
		Tc	Cr	Fe
1M NaOH	1	12002	[redacted]	0.011
	100	1200		40.04
OG	1	1200	1100	0.1010
	100	1200	1100	0.09
1M NaOH + Cr	0	[redacted]	500	0.09
	1	500	700	0.09
	100	100	600	0.08
LAW	0	[redacted]	500	0.14
	1	900	900	0.45
	100	700	900	0.34

In the 1M NaOH control system, early removal of Tc proceeds at the maximum rate recorded (1200 % – hr^{-1}) regardless of the initial Tc concentration, 1 or 100 ppm. Upon introduction of Cr (1570 ppm, 1M NaOH + Cr simulant), Tc removal rate decreases ~~from 12 hr^{-1}~~ to 500 % – hr^{-1} (1 ppm Tc) and 100% – hr^{-1} (100 ppm Tc). The difference in Tc removal rate between starting Tc concentrations suggests that the effect of co-mingled Cr is dependent on the Tc concentration. Since $Fe(OH)_2(s)$ is expected to undergo a dissolution-oxidation-recrystallization process~~,~~[19,28] ~~releasing~~ that releases Fe(II) into solution, Cr may scavenge $Fe(II)_{aq}$ thus limiting surface Fe(II) capable of heterogeneously reducing Tc. With Tc present, $Fe(OH)_2(s)$ dissolution increases and is consumed by Cr, translating into an increase in Cr removal rates, from 500 % – hr^{-1} (1M NaOH + Cr, no Tc) to 600 % – hr^{-1} (100 ppm Tc) and 700 % hr^{-1} (1 ppm Tc). Therefore, until $Fe(II)_{aq}$ oxidizes and recrystallizes or $Fe(II)_{aq}$ sorbs to a mineral surface, Tc removal (and likely reduction) will remain slower than Cr removal.— A similar trend was also observed in the LAW simulant (Error: Reference source not foundD), where Cr removal rate increased from 500 % – hr^{-1} (no Tc) to 900 % hr^{-1} when 1 or 100 ppm Tc is present, suggesting the additional ions in the simulant negate the Tc concentration dependence on Cr removal rate. The release rate of Fe into LAW also increased by up to ~3× compared to the Fe release rate in LAW without Tc, potentially providing additional $Fe(II)_{aq}$ for homogeneous reduction of Cr. Curiously, Tc removal rates in the LAW system are higher relative to the 1M NaOH + Cr system: 700% hr^{-1} at 100 ppm Tc and 900% hr^{-1}

at 1 ppm Tc. This increase in Tc removal rates may be due to the decrease in total Cr in the system from 1570 ppm (1M NaOH + Cr) to 1080 ppm (LAW). Additionally, the presence of complexing ions, such as SO_4^{2-} and NO_3^-, facilitate faster $Fe(OH)_2(s)$ dissolution, as evidenced by the increase in Fe released into solution over the initial 0.08 hr (Table 2). SO_4^{2-} and NO_3^- are also ~~oxidizes~~oxidizers, ~~such~~ which promote oxidation and recrystallization, providing additional surface area for Fe(II) sorption and heterogeneous reduction of Tc.[23,28]

Finally, in the OG simulant Tc and Cr removal proceeds rapidly at rates of 1200% hr^{-1} and 1100% hr^{-1}, respectively, due to the drop in pH (from >13 to 5.6) resulting in a decrease in oxidation of $Fe(II)_{aq}$ oxidation by dissolved oxygen, lower Cr concentrations (down to 90 ppm), and other co-mingled constituent concentrations, e.g. SO_4^{2-}, which is known to complex with Fe(II) ions and increase solid dissolution and nucleation.[23,28] This OG simulant environment may provide the necessary conditions to simultaneously promote both homogeneous and heterogeneous reduction, such that both Tc and Cr are eventually removed at similar rates.

Early Solid Phase Formation and Mineralogical Characterization. In addition to rapid removal of Tc and Cr, the amount of Fe released into solution during the initial 0.08 hour of reaction is only a small fraction (≤4 %) of the available Fe in the system, suggesting that (i) $Fe(II)_{aq}$ oxidation is occurring, and (ii) reaction products are being formed (Supporting Information (SI), Table S1). Following reduction of Cr(VI) and Tc(VII), several

potential pathways are expected to contribute to their removal and stabilization, including Cr(III) and Tc(IV) incorporation into iron spinels (e.g., magnetite [Fe_3O_4] and chromite [$FeCr_2O_4$]),[1,10-12,29-35] iron oxyhydroxides (e.g., goethite [α-FeOOH] and feroxyhyte [δ-FeOOH]),[1,4,7,36-38] or the formation of other oxide and hydroxide phases, e.g. $TcO_2{\cdot}xH_2O$ and $Cr(OH)_3$.[13,16,39-42] However, formation of the final solid product is highly dependent on the simulant chemistry[23,28,43-45] and the nature of the final product is critical to assessing the fate of Tc and Cr. X-ray diffraction (XRD) patterns collected from select solids after reaction in Tc-free simulants were used to quantify the distribution of mineral phases and identify mineralogical differences as a function of simulant chemistry (Error: Reference source not found, Error: Reference source not found). Little change in the final mineralogical composition is expected in Tc-containing solids due to the relatively low Tc concentrations studied and the negligible change in calculated lattice parameters, indicative of contaminant substitution, expected upon Tc(IV) substitution for Fe(III) due to their identical crystal radii, 0.785 Å.[7,32,33]

Table 3. Solid Mineralogy Determined by XRD Pattern Analysis[(a)]

Simulant	pH	Spinel *a* parameter,[(b)] Å	Spinel	Goethite [α-FeOOH]	Feroxyhyte [δ-FeOOH]	Amorph.
1M NaOH[(c)]	13.5	8.394(1)	27%	25%	8%	40%
1M NaOH + Cr	13.5	8.3840(4)	30%	34%	25%	11%
Off-Gas	5.6	8.4038(2)	95%	-	-	5%
LAW[(d)]	13.5	-	-	77%	17%	6%

[(a)]XRD samples do not contain Tc.
[(b)] Reference spinel *a* parameters: magnetite [Fe_3O_4] = 8.396 Å, chromite [$FeCr_2O_4$] =

8.378 Å, and maghemite [γ-Fe_2O_3] = 8.34 Å.[46,47] Values in parentheses indicate the standard deviation of the last decimal place.
[(c)] As reported by Saslow et al. 2017[11]
[(d)] As reported by Saslow et al. 2018[6]
-: Not Detected

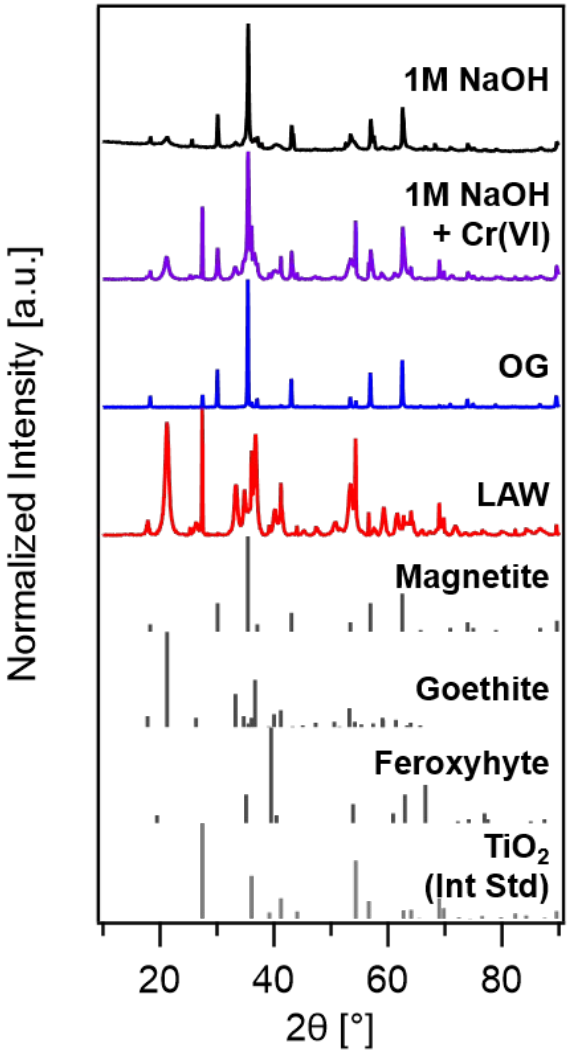

Figure 2. XRD diffraction patterns for solids formed in 1M NaOH (black), 1M NaOH + Cr (purple), OG Simulant (blue), and LAW Simulant (red). Standard diffraction peak intensities for magnetite (Fe_3O_4), goethite (α-FeOOH), feroxyhyte (γ-FeOOH), and the TiO_2 internal standard shown in grey.

From analysis of the XRD patterns, the impact of pH on the minerals produced in the solid phase is immediately apparent: 95% of the solid formed in the OG simulant (pH 5.6) consists of iron spinel, primarily as magnetite based on the lattice *a* parameter (8.4038 Å). Magnetite is favorably formed via co-precipitation of aqueous Fe(III) and Fe(II) ions, provided that the ratio of Fe(III) to (Fe(III) + Fe(II)) is ~0.66, and that the OH/ Fe_{total} ratio is > 2.[48] At lower pH, $Fe(II)_{aq}$ oxidation by dissolved oxygen is slower, though homogeneous reduction of Cr in the OG would increase $Fe(II)_{aq}$ oxidation rates. These two competing processes may maintain the desired fraction of $Fe(III)_{aq}$ needed to primarily form magnetite.

When the pH of the simulant is increased to 13.5, the mineral phases present in the reaction product are dominated by iron oxyhydroxide phases rather than spinels, as $Fe(II)_{aq}$ oxidation occurs more rapidly. For instance, in the 1M NaOH simulant without Cr, magnetite accounts for only 27% of the reaction product, based on the measured spinel *a* parameter (8.394 Å).[46,47] The remaining solid consists of 33% iron oxyhydroxides (goethite and feroxyhyte) and 40% amorphous material. Upon Cr addition to 1M NaOH, the amount of amorphous material in the solid drops from 40% to 11% with a subsequent increase in spinel (30%), goethite (34%) and feroxyhyte (25%) contributions. The spinel *a* parameter also decreases to 8.384 Å, a value that falls between reported values for magnetite and chromite/maghemite, that suggests either magnetite is oxidizing and forming maghemite or Cr is being incorporated into the spinel phase[46,47] thus reducing the spinel *a* parameter

362 due to the smaller crystal radius of Cr(III), 0.755 Å, compared to Fe(III), 0.785
363 Å. However, Cr(III) is likely incorporated to some degree into all of the
364 detected Fe(III)-bearing phases. [40,41,49-52]

365 In the LAW simulant, the reaction product was 94% iron oxyhydroxides,
366 with the remainder being amorphous material. SO_4^{2-} and Cl^- have been
367 previously reported to drive the formation of goethite (α-FeOOH) and other
368 polymorphs of FeOOH depending on their concentration and ~~if~~ whether they
369 are co-mingled.[43,44] Additionally, NO_3^- in the presence of oxygen has also
370 been shown to drive the formation of goethite.[19,45] Since the LAW simulant
371 has the highest concentration of SO_4^{2-} and NO_3^- ~~–~~ of the four simulants tested,
372 the lack of spinel phases in the solid is expected. Furthermore, since the 1M
373 NaOH and 1M NaOH + Cr simulants do not contain SO_4^{2-} and other redox
374 competitive anions, the formation of spinel phases at a detectable level
375 remains feasible despite alkaline conditions, pH ~13.5. Finally, the low pH of
376 the OG simulant likely overcomes any mineralogical impact caused by the
377 presence of SO_4^{2-} in the OG, although the SO_4^{2-} concentration in the OG is
378 ~75% less than in LAW, so would have a lesser impact on mineralogy in this
379 system regardless of pH.

380 *Late Constituent Removal (0.08 – 24 hours).* With nearly all Fe
381 associated with the final solid phase ~~within~~ after 0.08 hours (5 minutes),
382 solution phase reduction and removal processes are limited for Tc and Cr
383 after 0.08 hours. As a result, the solid mineralogy, simulant chemistry, and
384 preference towards heterogenous vs. homogeneous reduction pathways play

a greater role in the reduction and removal of the remaining Tc and Cr. Across all four simulants, key changes in Tc and Cr removal occurred between 0.08 – 1 hour and 1 – 24 hours. The transition at 1 hour also correlates with the approximate time required for complete $Fe(OH)_2(s)$ transformation.[28,43-45] To quantify changes in removal rate, Table S2 provides second order rate constants determined for each time period and constituent. Whereas previous studies show that Tc reduction occurs via a pseudo first order reaction,[14-16] the reaction kinetics for the more complex, multi-component simulant solutions studied here can be better described using a second order rate model for Tc, Cr, and Fe. These rate constants were determined from a linear fit to the data, plot as $1/[M/M_0]$ vs. time, where M represents Tc, Cr, or Fe and M_0 is the initial concentration in the system for that constituent.

As a first example of how the solid phase and reduction mechanisms influence the rate of Tc and Cr removal within 0.08 – 1 hour, the inset plot in Error: Reference source not foundC shows that Tc is preferentially removed over Cr within the OG simulant. Considering that the solid formed is 95% magnetite, electron-shuttling between Fe(II)/Fe(III) sites near the magnetite surface are capable of heterogeneously reducing Tc, likely at a rate similar or faster than homogenous reduction Cr in solution. As a result, Tc removal is complete before or in parallel with Cr. Furthermore, incorporation into magnetite is more favorable for Tc than Cr, due to Tc(IV) sharing an identical crystal radius with Fe(III) that makes incorporation into the iron oxide phase

energetically more favorable. [7,32,33] After 1 hour has passed, less than 1 ppm of Tc and Cr remain in the system, and a decrease in removal rate is observed, likely due to Le Chatelier's principle.

In the 1M NaOH simulant, 92 – 93% of Tc is removed within the first 0.08 hours of reaction and 27% of the solid formed is magnetite. Similar to the OG samples, Tc removal continues to completion by the end of the 24 hour period; however, within the 0.08 – 1 hour time period, Tc removal from the 100 ppm Tc system stops whereas the 1 ppm Tc system continues nearer to complete removal. In the 1M NaOH system only, these observations in Tc removal rates inversely correlate with Fe removal rates (SI Table S2). As Tc is heterogeneously reduced at the magnetite surface, Fe removal may be slowed if Tc occupies sorption sites also used for Fe(II)/Fe(III) electron transfer and mineral growth. This scenario may explain the decrease in Fe removal rate as Tc removal in the 1 ppm Tc system continues, as well as the inverse observed in the 100 ppm Tc system, where Fe removal rate increases and Tc removal decreases within the 0.08 – 1 hour period.

The most striking impact that the nature of the reaction product has on the fate of Tc and Cr in solution is observed when comparing the 1M NaOH + Cr and LAW simulants. In each of these simulants, the removal rate of Cr within the 0.08 – 1 hour time period is orders of magnitude slower than Cr removal rates from the OG simulant and consistently lower than the associated co-mingled Tc removal rates (SI Table S2). In fact, when

observing Error: Reference source not foundB and Error: Reference source not foundD, Cr removal appears to stall during this period while Tc removal continues. During this time the solid surface mediated reduction of Tc(VII), which is more favorable than heterogeneous Cr(III) reduction, presumably continues and Tc is removed from solution. Furthermore, with less Fe(II) available in solution, Cr(VI) reduction is likely hindered. After 1 hour, the presence of structural Fe(II) in magnetite, found in the solid phase formed within the 1M NaOH + Cr simulant, allows for Tc(VII) removal to proceed in parallel with Cr(VI) removal until completion. Due to the increase in Tc concentration, the 100 ppm Tc spiked 1M NaOH + Cr simulant takes longer to achieve complete removal of Tc compared to the 1 ppm spiked simulant. This is in contrast with the LAW simulant, where Tc(VII) reduction likely ceases after one hour in the absence of magnetite, and Tc is not completely removed within the 24 hour reaction period. Yet with the cessation of Tc removal, Cr removal rates continuously increase and complete Cr removal is achieved after 24 hours. This trend in Cr removal suggests that the additional Fe in solution determined from the sub-sample taken at 1 hour (SI Table S1) provides $Fe(II)_{aq}$ that continues to facilitate Cr(VI) homogeneous reduction and removal.

Speciation of Cr and Tc in the Bulk Solid Phase. As alluded to in the discussion of the XRD results, the removal of Tc and Cr from solution occurs through the formation of a solid phase and partial or complete incorporation into one of the iron oxide or oxyhydroxide phases formed (Table 3). To

explore which reduction pathways are influential in the removal of Cr and Tc from each simulant, the speciation of Tc and Cr was determined using X-ray absorption near edge structure (XANES) spectroscopy on the solids collected from the 100 ppm Tc batch experiments. In Table 4, the fractional distribution of Tc and Cr species are provided for each simulant. These values were determined from linear combination fits to the XANES spectra shown in Figure 3. Procedures for fitting XANES spectra using liner combination analysis (LCA) and standards used are provided in the SI.

Speciation trends from Tc K-edge XANES spectra and LCA fits align well with Tc removal rates and reaction product compositions. The amount of $Tc(VII)O_4^-$ associated with the reaction product was minimal (≤8 %) in spinel-containing solids, as would be expected for Tc completely removed from these simulants by reduction-mediated processes. Some $Tc(VII)O_4^-$ (28 %) is present in the reaction product from the LAW simulant, in which Tc removal was not complete. However, only 8 – 14 % of Tc remained in the LAW simulant after 24 hrs. With twice as much $Tc(VII)O_4^-$ in the solid analyzed by XANES, in addition to trace fractions of $Tc(VII)O_4^-$ in solids from simulants achieving complete Tc removal, some reoxidation of Tc(IV) between sample preparation and analysis may have occurred.

In general, the amount of Tc(IV) associated with magnetite in the Tc K-edge XANES spectra increased in parallel with the amount of magnetite present in the reaction product, as determined by XRD. Although no magnetite was detected in the reaction product from the LAW simulant by

XRD, the 11 % of Tc-incorporated magnetite in the Tc K-edge XANES could represent Tc(IV) replacing Fe(III) in an ordered octahedral environment in goethite, which accounts for 77 % of the reaction product by XRD. Tc-incorporated magnetite accounts for 61% of Tc in the OG sample, corresponding with magnetite forming 95% of the reaction product by XRD. For the 1 M NaOH simulants (with and without Cr) ~40 – 50% of Tc is associated with the mixed spinel/oxyhydroxide/amorphous phases as Tc-incorporated magnetite. The remaining Tc in each was present as $Tc(IV)O_2{\cdot}xH_2O$, formed as Tc(VII) was reduced at the solid surface, but not incorporated into the magnetite or iron oxyhydroxide mineral structure. $Tc(IV)O_2{\cdot}xH_2O$, which is more susceptible to reoxidation than Tc(IV) incorporated iron (oxyhydr)oxides, is the phase most likely to reoxidize between sample preparation and analysis, inflating the fraction of $Tc(VII)O_4^-$ found in the solid.

Cr speciation in the solids analyzed also support the proposed kinetic pathways. As with $Tc(VII)O_4^-$, very little (<1%) $Cr(VI)O_4^{2-}$ was present in the reaction product, supporting the requirement that Cr(VI) reduction to Cr(III) must occur to remove Cr from solution. In all of the simulants 30 – 40% of Cr(III) adopts a disordered coordination environment, even in the OG simulant where 95% of the reaction product is magnetite. This supports the hypothesis that reduction of Cr(VI) to Cr(III) is not associated with the Fe-bearing mineral phase, and occurs in solution to produce a disordered

499 $Cr(OH)_3$ or amorphous phase, which may subsequently form a protective
500 layer on the exterior of the Fe-bearing minerals.

501 The distribution of the remaining Cr(III) between chromite ($Fe_2Cr(III)O_4$)
502 and partial incorporation into an inverse spinel phase ($Fe_{2.5}Cr(III)_{0.5}O_4$)
503 demonstrates how simulant chemistry influences Cr(III) incorporation into the
504 solid. In the OG simulant, where there is minimal competition from other
505 constituents and the pH is 5.6,—the remaining Cr(III) is present as $Fe_2Cr(III)O_4$
506 (30%), with some partial incorporation in $Fe_{2.5}Cr(III)_{0.5}O_4$ (25%), although an
507 insufficient quantity to influence the magnetite lattice parameter (Table 3).
508 Thus, while homogeneous reduction of Cr(VI) dominates, these results
509 suggest that some heterogeneous reduction of Cr(VI) by the Fe-bearing
510 mineral phase may occur in the OG. Alternatively, disordered Cr(III) phases
511 that precipitate on mineral surfaces may become incorporated into the
512 magnetite crystal structure as mineral transformation continues. As the pH
513 and Cr concentration increase in the 1M NaOH + Cr simulant, $Fe_2Cr(III)O_4$ only
514 contributes 12% to the reaction product, with 44% of Cr(III) partially
515 incorporated into $Fe_{2.5}Cr(III)_{0.5}O_4$. However, with this technique it is difficult to
516 distinguish between Cr(III) incorporated into ordered octahedral sites in
517 magnetite or in goethite. For the LAW simulant, 51 % of the Cr(III) is
518 incorporated into an ordered iron oxyhydr(oxide).

519 **Table 4.** Solid Phase Tc and Cr Speciation as Determined from LCA of XANES
520 Spectra

Simulant	1M NaOH	1M NaOH + Cr	OG	LAW
		Cr XANES		

Cr(III) Alum		0.30(2)	0.36(3)	0.40(2)
$Fe_{2.5}Cr(III)_{0.5}O_4$		0.44(2)	0.25(4)	0.51(2)
$FeCr(III)_2O_4$		0.12(1)	0.30(3)	0.05(1)
$Cr(III)_2O_3$		-	-	-
$K_2Cr(VI)O_4$		0.009(3)	0.01(1)	0.000(3)
Tc XANES				
$Tc(VII)O_4^-$	0.08(1)	0.079(4)	0.032(4)	0.28(1)
$Tc(IV)O_2{\cdot}xH_2O$	0.47(6)	0.40(4)	0.34(5)	0.61(5)
Tc(IV)-Magnetite	0.44(5)	0.51(4)	0.61(5)	0.11(5)

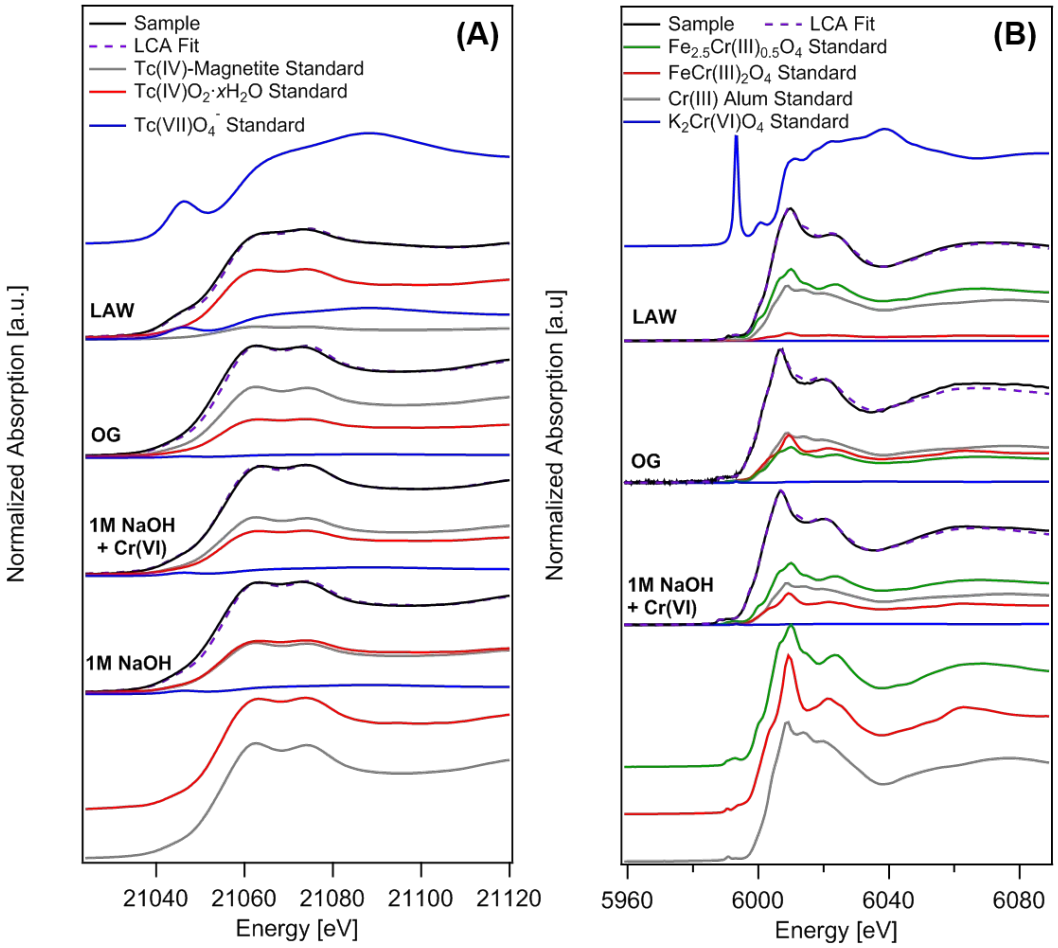

Figure 3. (A) Tc K-edge XANES spectra collected from the final solid phase reacted in 1M NaOH, 1M NaOH + Cr, OG Simulant, and LAW Simulant (black traces). LCA fits (purple, dashed) determined from TcO_4^- (blue), $TcO_2{\cdot}xH_2O$ (red), and Tc-Magnetite (grey) standards. The fraction of each Tc standard contributing to the LCA fit is shown in the corresponding color under each sample. (B) Cr K-edge XANES spectra collected from the final solid phase reacted in 1M NaOH + Cr, OG Simulant, and LAW Simulant (black traces). LCA fits (purple, dashed) determined from $Fe_{2.5}Cr(III)_{0.5}O_4$ (green), $FeCr(III)_2O_4$ (chromite, red), Cr(III) Alum (grey), and $K_2Cr(VI)O_4$ (blue) standards. The

fraction of each Cr standard contributing to the LCA fit is shown in the corresponding color under each sample.

Local Coordination Environment of Tc in the Solid Phase: The local coordination environment of Tc, e.g. bond lengths between neighboring atoms and coordination number, offers additional insight into Tc speciation and incorporation into the final solid product that cannot be provided by XANES. EXAFS spectra of the reaction products were interpreted using a shell-by-shell fitting approach in ARTEMIS[27] to determine which scattering pathways contribute to the fit. Based on previous work, goethite (LAW sample only),[1,38,53] magnetite,[1,54] $TcO_2 \cdot 2H_2O$,[55] and TcO_4^-,[36] models were considered when fitting EXAFS spectra. The results of these fits and the models used are shown in Table 5 and the EXAFS spectrum and fit for each sample shown in Figure 4. The spectra shown for the LAW and 1 M NaOH +Cr simulant solids have been previously published,[6,11] but were refit here under fitting constraints consistently used across all four samples for better comparison.

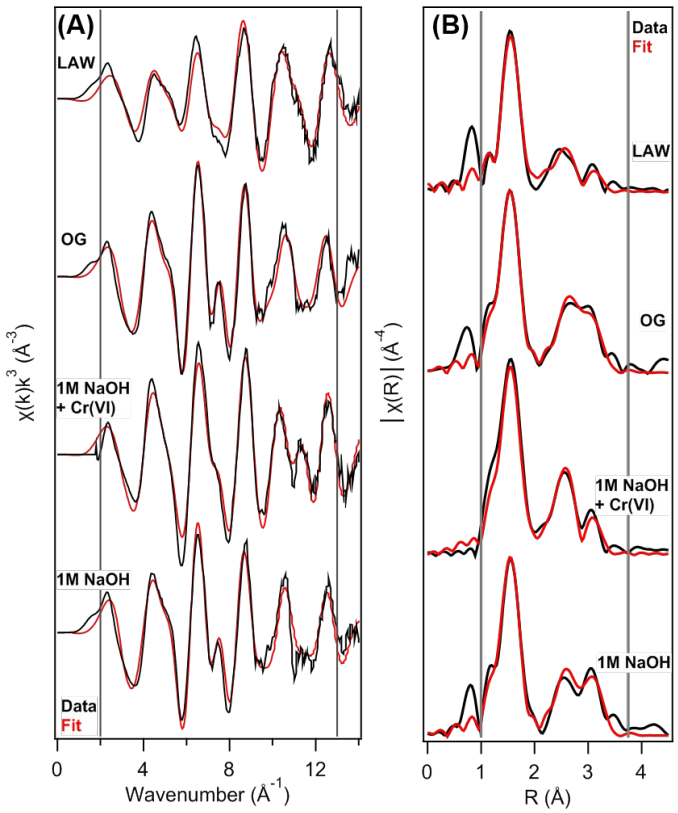

549

550 **Figure 4.** EXAFS spectra (A) and their Fourier transforms (B) for Tc-
551 containing solids formed in 1 M NaOH, 1 M NaOH + Cr, OG Simulant, and
552 LAW Simulant. All starting solutions initially contained 100 ppm Tc. EXAFS
553 fits (red) to the data (black) are based on a combination of Tc-incorporated
554 magnetite, Tc-incorporated goethite, $TcO_2 \cdot 2H_2O$, and TcO_4^- models.

555

Table 5. Tc EXAFS Fit Parameters[a]

Sample	Neighbor Atoms	CN	R + ΔR (Å)	σ^2	p(F)	ΔE_0	R Factor
LAW[6,b] (Refit spectrum from Saslow et al. 2018)	$O_{Tc(VII)}$	1.2(1)	1.72*	0.001*	<0.001	0(2)	0.021
	O	4.2(1)	2.02(1)	0.004(1)	<0.001		
	Tc_{TcO2}	1.0(1)	2.59(1)	0.007(1)	0.001		
	Fe_{Oh}	1.4(1)	3.06(2)	0.007(1)	0.006		
	Fe_{Td}	1.4(1)	3.55(3)	0.008(3)	<0.001		
OG[c]	O	6*	2.021(4)	0.004(3)	<0.001	0.7(9)	0.014
	Fe_{Oh}	5*	3.07(1)	0.010(1)	<0.001		
	Tc_{Oh}	1*	3.07(1)	0.010(1)			
	Fe_{Td}	6*	3.50(1)	0.010(1)	<0.001		
1M NaOH + Cr[11,c] (Refit Spectrum from Saslow et al. 2017)	O	6*	2.02(1)	0.003(1)	<0.001	1(2)	0.037
	Tc_{TcO2}	1.1(1)	2.59(1)	0.006(1)	0.001		
	Fe_{Oh}	2.7(2)	3.03(1)	0.006(1)	<0.001		
	Fe_{Td}	2.7(2)	3.52(4)	0.007(3)	0.001		
1M NaOH[c]	O	6*	2.02(1)	0.004(1)	<0.001	2(1)	0.036
	Fe_{Oh}	4*	3.07(2)	0.006(2)	0.001		
	Tc_{Oh}	2*	3.07(2)	0.006(2)			
	Fe_{Td}	6*	3.52(1)	0.010(1)	<0.001		
Goethite[1,38,53]	O	6	1.95-2.09				
	Fe_{Oh}	4	3.01 – 3.28				
	Fe_{Td}	4	3.59				
Magnetite[1,54]	O	6	2.06				
	Fe_{Oh}	6	2.97				
	Fe_{Td}	6	3.48				
$TcO_2 \cdot 2H_2O$[55]	O	4	2.06				
	O	2	2.47				
	Tc	2	2.57				
TcO_4^-,[36]	O	4	1.72				

[a] S_o^2= 0.8; coordination number (CN); k space fit window 2 – 13, Fourier transform fit window 1 – 3.75; interatomic distance (R + ΔR); disorder parameter (σ^2); energy shift (ΔE^0); goodness of fit parameter (R-factor); F-test [p(F)]. A F-test was performed on each scattering shell to determine the best model.[56] If the probability of F [p(F)] is less than 0.05, the addition of that shell improves the fit to greater than 2σ and that shell was considered to be observed in the experiments. [b] Goethite model used for iron-containing mineral phase. [c] Magnetite used for iron-containing mineral phase. *Fixed Value.

The EXAFS data for three of the simulants could be fit with Tc(IV) incorporated into a magnetite model. Only the reaction product from the LAW simulant showed evidence for Tc incorporated into goethite. This is

again consistent with interpretations of the corresponding XRD and XANES data. Furthermore, the LAW simulant produced the only reaction product where TcO_4^- was required in the EXAFS fit, and it was present at the same relative concentration as observed in the XANES spectrum. In TcO_4^- , four oxygen atoms are located at ~1.72 Å from the central Tc atom. The presence of 1.2(1) oxygen atoms at this bond distance for the Tc in the LAW reaction product suggests that ~30% of Tc has four nearest-neighbor oxygens (28 % of the Tc was present as TcO_4^- according to the LCA fit of the Tc K-edge XANES). The majority of the remaining Tc is present as Tc(IV) in $TcO_2 \cdot 2H_2O$ (~50%). With such a low association of Tc with the iron-bearing mineral phase, Tc present in the LAW solid could be more susceptible to reoxidation.

For the remaining three simulants, OG, 1M NaOH, and 1M NaOH + Cr, clear trends in the number of Tc atoms incorporated into Fe(III) sites offer clues as to how these solids were formed. Tc(IV) and Cr(III) readily substitute for Fe(III), so substitution of Tc and Cr into a nearest neighboring Fe(III) site is considered in the EXAFS fit. In the case of the 1 M NaOH + Cr simulant, including Tc and Cr as nearest neighbors did not significantly improve the fit. An improvement was only achieved by including a neighboring Tc atom with a bond length of ~2.59 Å, typical of $TcO_2 \cdot 2H_2O$. In the OG and 1 M NaOH simulant, including neighboring Tc atoms from $TcO_2 \cdot 2H_2O$ did not improve the fit, whereas including Tc atoms in neighboring Fe(III) sites significantly improved the fit to the EXAFS data. In the 1 M NaOH simulant, Cr is not

present to compete with Tc incorporation into magnetite, and two Tc atoms may be incorporated as nearest neighbors. When Cr is introduced, but at a lower pH in the OG simulant, Tc incorporation into neighboring Fe(III) sites occurs to a lesser extent.

4. Conclusions

The removal of Tc by $Fe(OH)_2(s)$, in the presence of Cr, and under various waste simulant conditions, has been demonstrated previously. In this work, novel kinetic information provides context to the success of $Fe(OH)_2(s)$ and the fate of Tc (and Cr) in the reaction products. One key observation is the rate of $Fe(OH)_2(s)$ dissolution-oxidation-recrystallization, and early removal of Tc and Cr from solution. In nearly all of the simulants studied, 40 – 96% of Tc and/or Cr are removed within the first five minutes after addition of $Fe(OH)_2(s)$ to the simulant. This implies that rapid addition of $Fe(OH)_2(s)$ into the waste stream and homogenization of the suspension is essential for effective treatment. Additionally, the pH, co-mingled constituents, and contaminant concentrations will play a key role in determining the final $Fe(OH)_2(s)$ transformation product, with incorporation of Tc(IV) into spinels, such as magnetite, favored by low pH simulants, e.g. OG simulant pH 5.6, and lower co-mingled Cr and other constituent concentrations, e.g. 1 M NaOH simulant. With the higher pH simulants, e.g. > pH 13, less magnetite is formed and oxyhydroxides, including goethite, are in some cases the favored product. As a result, the incorporation of Tc(IV) into the iron oxide/oxyhydroxide phase decreases and ~~rather~~ TcO_4^- forms $TcO_2 \cdot 2H_2O$ once

606 reduced. Finally, the remaining Tc and/or Cr in the waste simulants studied
607 here reached steady-state removal within 24 hours. Only in the LAW
608 simulants was complete removal of Tc not reached within this time period.
609 Since Tc favors a heterogeneous reduction process that occurs on a solid
610 surface as opposed to homogeneous reduction by dissolved Fe(II) (favored
611 by Cr(VI)), Tc is primarily removed in the first hour, during which Cr removal
612 ceases in systems with high pH and high Cr concentrations (1M NaOH + Cr
613 and LAW simulants). This also coincides with the approximate time required
614 for the final solid iron oxide/oxyhydroxide product to form, thus limiting long-
615 term reduction and removal processes that rely on the $Fe(OH)_2(s)$
616 transformation mechanism. In these two simulants Cr removal resumes
617 between 1 – 24 hours.

618 With such diverse waste stream chemistries to be treated at the Hanford
619 Site, understanding how a treatment technology may perform differently in
620 these waste streams when targeting specific contaminants is critical for
621 evaluating possible implementation at the site. The results presented here
622 demonstrate the variable efficacy of $Fe(OH)_2(s)$ for Tc reduction and removal
623 from simulated waste streams with varying concentrations of co-mingled
624 redox competitors, including Cr. Reduction pathways, simulated waste
625 chemistry, and the mineralogical composition of the solid phase are key
626 drivers in determining Tc removal rate and total Tc removed, and are
627 expected to play a role in future work understanding how these materials
628 age and in the process release Tc through Tc(IV) reoxidation.

5. Acknowledgements

This research was supported by the U.S. Department of Energy's (DOE) Waste Treatment and Immobilization Plant Project of the Office of River Protection. PNNL is operated for the DOE by Battelle Memorial Institute under Contract DE-AC05-76RL0 1830. The XANES and EXAFS data collection was carried out at the SSRL with help from Ryan Davis. Use of the Stanford Synchrotron Radiation Lightsource, SLAC National Accelerator Laboratory, is supported by the U.S. Department of Energy, Office of Science, Office of Basic Energy Sciences under Contract No. DE-AC02-76SF00515. A portion of this work (WWL) was supported by the U.S. Department of Energy, Office of Science, Basic Energy Sciences, Chemical Sciences, Biosciences, and Geosciences Division (CSGB), Heavy Element Chemistry Program at Lawrence Berkeley National Laboratory under contract No. DE-AC02-05CH11231. A portion of this research was also supported by the National Research Foundation of Korea (NRF) grant funded by the Korean government (No. NRF-2017M2B2B1072374 and NRF-2017M2B2B1072404). The authors also wish to thank Guohui Wang for his valuable review and feedback on this work and Erin McElroy for assisting with batch experiments.

6. References

(1) Um, W.; Luksic, S. A.; Wang, G.; Saslow, S.; Kim, D.-S.; Schweiger, M. J.; Soderquist, C. Z.; Bowden, M. E.; Lukens, W. W.; Kruger, A. A. Enhanced 99Tc retention in glass waste form using Tc(IV)-incorporated Fe minerals. *Journal of Nuclear Materials.* **2017**, *495*, 455. https://doi.org/10.1016/j.jnucmat.2017.09.007.

(2) Kim, D.; Kruger, A. A. Volatile species of technetium and rhenium during waste vitrification. *Journal of Non-Crystalline Solids.* **2018**, *481*, 41. https://doi.org/10.1016/j.jnoncrysol.2017.10.013.
(3) Darab, J. G.; Smith, P. A. Chemistry of technetium and rhenium species during low-level radioactive waste vitrification. *Chemistry of Materials.* **1996**, *8*, 1004.
(4) Luksic, S. A.; Riley, B. J.; Schweiger, M.; Hrma, P. Incorporating technetium in minerals and other solids: A review. *Journal of Nuclear Materials.* **2015**, *466*, 526. http://dx.doi.org/10.1016/j.jnucmat.2015.08.052.
(5) Banerjee, D.; Kim, D.; Schweiger, M. J.; Kruger, A. A.; Thallapally, P. K. Removal of TcO4(-) ions from solution: materials and future outlook. *Chemical Society reviews.* **2016**, *45*, 2724. 10.1039/c5cs00330j.
(6) Saslow, S. A.; Um, W.; Pearce, C. I.; Bowden, M. E.; Engelhard, M. H.; Lukens, W. L.; Kim, D. S.; Schweiger, M. J.; Kruger, A. A. Cr(VI) Effect on Tc-99 Removal from Hanford Low-Activity Waste Simulant by Ferrous Hydroxide. *Environ Sci Technol.* **2018**, *52*, 11752. 10.1021/acs.est.8b03314.
(7) Smith, F. N.; Taylor, C. D.; Um, W.; Kruger, A. A. Technetium incorporation into goethite (α-FeOOH): An atomic-scale investigation. *Environmental Science & Technology.* **2015**, *49*, 13699. 10.1021/acs.est.5b03354.
(8) Smith, F. N.; Um, W.; Taylor, C. D.; Kim, D.-S.; Schweiger, M. J.; Kruger, A. A. Computational investigation of technetium(IV) incorporation into inverse spinels: Magnetite (Fe_3O_4) and trevorite ($NiFe_2O_4$). *Environmental Science & Technology.* **2016**, *50*, 5216. 10.1021/acs.est.6b00200.
(9) Um, W.; Chang, H.; Icenhower, J. P.; Lukens, W. W.; Jeffrey Serne, R.; Qafoku, N.; Kukkadapu, R. K.; Westsik, J. H. Iron oxide waste form for stabilizing 99Tc. *Journal of Nuclear Materials.* **2012**, *429*, 201. 10.1016/j.jnucmat.2012.06.004.
(10) Wang, G.; Um, W.; Kim, D.-S.; Kruger, A. A. 99Tc immobilization from off-gas waste streams using nickel-doped iron spinel. *Journal of Hazardous Materials.* **2019**, *364*, 69. https://doi.org/10.1016/j.jhazmat.2018.09.064.
(11) Saslow, S. A.; Um, W.; Pearce, C. I.; Engelhard, M. H.; Bowden, M. E.; Lukens, W.; Leavy, II; Riley, B. J.; Kim, D. S.; Schweiger, M. J.; Kruger, A. A. Reduction and Simultaneous Removal of (99)Tc and Cr by Fe(OH)2(s) Mineral Transformation. *Environ Sci Technol.* **2017**, *51*, 8635. 10.1021/acs.est.7b02278.
(12) Lee, M. S.; Um, W.; Wang, G.; Kruger, A. A.; Lukens, W. W.; Rousseau, R.; Glezakou, V. A. Impeding (99)Tc(IV) mobility in novel waste forms. *Nat Commun.* **2016**, *7*, 12067. 10.1038/ncomms12067.
(13) Li, D.; Kaplan, D. I. Sorption coefficients and molecular mechanisms of Pu, U, Np, Am and Tc to Fe (hydr)oxides: a review. *J Hazard Mater.* **2012**, *243*, 1. 10.1016/j.jhazmat.2012.09.011.
(14) Cui, D.; Eriksen, T. E. Reduction of Pertechnetate by Ferrous Iron in Solution: Influence of Sorbed and Precipitated Fe(II). *Environmental Science & Technology.* **1996**, *30*, 2259. 10.1021/es9506263.

(15) Cui, D.; Eriksen, T. E. Reduction of Pertechnetate in Solution by Heterogeneous Electron Transfer from Fe(II)-Containing Geological Material. *Environmental Science & Technology.* **1996**, *30*, 2263. 10.1021/es950627v.
(16) Zachara, J. M.; Heald, S. M.; Jeon, B.-H.; Kukkadapu, R. K.; Liu, C.; McKinley, J. P.; Dohnalkova, A. C.; Moore, D. A. Reduction of pertechnetate [Tc(VII)] by aqueous Fe(II) and the nature of solid phase redox products. *Geochimica et Cosmochimica Acta.* **2007**, *71*, 2137. http://dx.doi.org/10.1016/j.gca.2006.10.025.
(17) Peretyazhko, T.; Zachara, J. M.; Heald, S. M.; Jeon, B. H.; Kukkadapu, R. K.; Liu, C.; Moore, D.; Resch, C. T. Heterogeneous reduction of Tc(VII) by Fe(II) at the solid–water interface. *Geochimica et Cosmochimica Acta.* **2008**, *72*, 1521. 10.1016/j.gca.2008.01.004.
(18) Qafoku, O.; Pearce, C. I.; Neumann, A.; Kovarik, L.; Zhu, M.; Ilton, E. S.; Bowden, M. E.; Resch, C. T.; Arey, B. W.; Arenholz, E.; Felmy, A. R.; Rosso, K. M. Tc(VII) and Cr(VI) Interaction with Naturally Reduced Ferruginous Smectite from a Redox Transition Zone. *Environmental Science & Technology.* **2017**, *51*, 9042. 10.1021/acs.est.7b02191.
(19) Blesa, M. A.; Matijević, E. Phase transformations of iron oxides, oxohydroxides, and hydrous oxides in aqueous media. *Advances in Colloid and Interface Science.* **1989**, *29*, 173. https://doi.org/10.1016/0001-8686(89)80009-0.
(20) Cui, D.; Eriksen, T. E. 1996. *Reduction of Tc(VII) and Np(V) in solution by ferrous iron A laboratory study of homogeneous and heterogeneous redox processes*. Sweden.
(21) Qafoku, N. P.; Dresel, P. E.; McKinley, J. P.; Liu, C.; Heald, S. M.; Ainsworth, C. C.; Phillips, J. L.; Fruchter, J. S. Pathways of Aqueous Cr(VI) Attenuation in a Slightly Alkaline Oxic Subsurface. *Environmental Science & Technology.* **2009**, *43*, 1071. 10.1021/es802658x.
(22) Eary, L. E.; Rai, D. Chromate removal from aqueous wastes by reduction with ferrous ion. *Environmental Science & Technology.* **1988**, *22*, 972. 10.1021/es00173a018.
(23) Eary, L. E.; Rai, D. Kinetics of chromate reduction by ferrous ions derived from hematite and biotite at 25 degrees C. *American Journal of Science.* **1989**, *289*, 180. 10.2475/ajs.289.2.180.
(24) Taylor-Pashow, K. M.; Nash, C. A.; Crawford, C. L.; McCabe, D. J.; Wilmarth, W. R. 2014. *Laboratory Scoping Tests Of Decontamination Of Hanford Waste Treatment Plant Low Activity Waste Off-Gas Condensate Simulant*. SRNL-STI--2013-00719, Savannah River Site, Aiken, South Carolina.
(25) Russell, R. L.; Westsik Jr, J.; Swanberg, D. J.; Eibling, R. E.; Cozzi, A.; Lindberg, M. J.; Josephson, G. B.; Rinehart, D. E. 2013. *Letter report: LAW simulant development for cast stone screening tests*.– Pacific Northwest National Laboratory, Richland, WA.
(26) Webb, S. M. SIXpack: a graphical user interface for XAS analysis using IFEFFIT. *Physica Scripta.* **2005**, *2005*, 1011.

(27) Ravel, B.; Newville, M. ATHENA, ARTEMIS, HEPHAESTUS: Data analysis for X-ray absorption spectroscopy using IFEFFIT. *Journal of Synchrotron Radiation.* **2005**, *12*, 537.
(28) Domingo, C.; Rodríguez-Clemente, R.; Blesa, M. A. Kinetics of oxidative precipitation of iron oxide particles. *Colloids and Surfaces A: Physicochemical and Engineering Aspects.* **1993**, *79*, 177. 10.1016/0927-7757(93)80173-c.
(29) Lukens, W. W.; Magnani, N.; Tyliszczak, T.; Pearce, C. I.; Shuh, D. K. Incorporation of technetium into spinel ferrites. *Environmental Science & Technology.* **2016**, *50*, 13160. 10.1021/acs.est.6b04209.
(30) Lukens, W. W.; Saslow, S. A. Facile incorporation of technetium into magnetite, magnesioferrite, and hematite by formation of ferrous nitrate in situ: precursors to iron oxide nuclear waste forms. *Dalton Transactions.* **2018**. 10.1039/C8DT01356J.
(31) Marshall, T. A.; Morris, K.; Law, G. T.; Mosselmans, J. F.; Bots, P.; Parry, S. A.; Shaw, S. Incorporation and retention of 99-Tc(IV) in magnetite under high pH conditions. *Environ Sci Technol.* **2014**, *48*, 11853. 10.1021/es503438e.
(32) Skomurski, F. N.; Rosso, K. M.; Krupka, K. M.; McGrail, B. P. Technetium Incorporation into Hematite (α-Fe_2O_3). *Environmental Science & Technology.* **2010**, *44*, 5855. 10.1021/es100069x.
(33) Smith, F. N.; Um, W.; Taylor, C. D.; Kim, D. S.; Schweiger, M. J.; Kruger, A. A. Computational Investigation of Technetium(IV) Incorporation into Inverse Spinels: Magnetite (Fe3O4) and Trevorite (NiFe2O4). *Environ Sci Technol.* **2016**, *50*, 5216. 10.1021/acs.est.6b00200.
(34) Jung, Y.; Choi, J.; Lee, W. Spectroscopic investigation of magnetite surface for the reduction of hexavalent chromium. *Chemosphere.* **2007**, *68*, 1968. http://dx.doi.org/10.1016/j.chemosphere.2007.02.028.
(35) Kendelewicz, T.; Liu, P.; Doyle, C. S.; Brown Jr, G. E. Spectroscopic study of the reaction of aqueous Cr(VI) with Fe_3O_4 (111) surfaces. *Surface Science.* **2000**, *469*, 144. http://dx.doi.org/10.1016/S0039-6028(00)00808-6.
(36) Pepper, S. E.; Bunker, D. J.; Bryan, N. D.; Livens, F. R.; Charnock, J. M.; Pattrick, R. A. D.; Collison, D. Treatment of radioactive wastes: An X-ray absorption spectroscopy study of the reaction of technetium with green rust. *Journal of Colloid and Interface Science.* **2003**, *268*, 408. http://dx.doi.org/10.1016/j.jcis.2003.08.024.
(37) Um, W.; Chang, H.; Icenhower, J. P.; Lukens, W. W.; Jeffrey Serne, R.; Qafoku, N.; Kukkadapu, R. K.; Westsik Jr, J. H. Iron oxide waste form for stabilizing ^{99}Tc. *Journal of Nuclear Materials.* **2012**, *429*, 201. http://dx.doi.org/10.1016/j.jnucmat.2012.06.004.
(38) Um, W.; Chang, H. S.; Icenhower, J. P.; Lukens, W. W.; Serne, R. J.; Qafoku, N. P.; Westsik, J. H.; Buck, E. C.; Smith, S. C. Immobilization of 99-technetium (VII) by Fe(II)-goethite and limited reoxidation. *Environ Sci Technol.* **2011**, *45*, 4904. 10.1021/es104343p.
(39) Heald, S. M.; Zachara, J. M.; Jeon, B.-H.; McKinley, J. P.; Kukkadapu, R.; Moore, D. In *X-Ray Absorption Fine Structure--XAFS 13* 2007; Vol. 882, p 173.

(40) Papassiopi, N.; Pinakidou, F.; Katsikini, M.; Antipas, G. S. E.; Christou, C.; Xenidis, A.; Paloura, E. C. A XAFS study of plain and composite iron(III) and chromium(III) hydroxides. *Chemosphere.* **2014**, *111*, 169. http://dx.doi.org/10.1016/j.chemosphere.2014.03.059.
(41) Papassiopi, N.; Vaxevanidou, K.; Christou, C.; Karagianni, E.; Antipas, G. S. E. Synthesis, characterization and stability of Cr(III) and Fe(III) hydroxides. *Journal of Hazardous Materials.* **2014**, *264*, 490. http://dx.doi.org/10.1016/j.jhazmat.2013.09.058.
(42) Pettine, M.; D'Ottone, L.; Campanella, L.; Millero, F. J.; Passino, R. The reduction of chromium (VI) by iron (II) in aqueous solutions. *Geochimica et Cosmochimica Acta.* **1998**, *62*, 1509. http://dx.doi.org/10.1016/S0016-7037(98)00086-6.
(43) Domingo, C.; Rodríguez-Clemente, R.; Blesa, M. A. Nature and reactivity of intermediates in the auto-oxidation of iron (II) in aqueous acid media. *Solid State Ionics.* **1993**, *59*, 187. https://doi.org/10.1016/0167-2738(93)90049-9.
(44) Domingo, C.; Rodríguez-Clemente, R.; Blesa, M. A. The pathways to spinel iron oxides by oxidation of iron (II) in basic media. *Materials Research Bulletin.* **1991**, *26*, 47. https://doi.org/10.1016/0025-5408(91)90037-M.
(45) Sugimoto, T.; Matijević, E. Formation of uniform spherical magnetite particles by crystallization from ferrous hydroxide gels. **1980**, *74*, 227. 10.1016/0021-9797(80)90187-3.
(46) Deer, W. A.; Howie, R. A.; Zussman, J. *An introduction to the rock-forming minerals*; 3 ed.; The Mineralogical Society: London, UK, 2013.
(47) Gorski, C. A.; Scherer, M. M. Determination of nanoparticulate magnetite stoichiometry by Mössbauer spectroscopy, acidic dissolution, and powder X-ray diffraction: A critical review. *American Mineralogist.* **2010**, *95*, 1017.
(48) Jolivet, J.-P.; Chanéac, C.; Tronc, E. Iron oxide chemistry. From molecular clusters to extended solid networks. *Chemical Communications.* **2004**, 481.
(49) Sass, B. M.; Rai, D. Solubility of amorphous chromium(III)-iron(III) hydroxide solid solutions. **1987**, *26*, 2228. 10.1021/ic00261a013.
(50) Schwertmann, U.; Gasser, U.; Sticher, H. Chromium-for-iron substitution in synthetic goethites. *Geochimica et Cosmochimica Acta.* **1989**, *53*, 1293. https://doi.org/10.1016/0016-7037(89)90063-X.
(51) McCarty, K. F.; Boehme, D. R. A Raman study of the systems $Fe_{3-x}Cr_xO_4$ and $Fe_{2-x}Cr_xO_3$. *Journal of Solid State Chemistry.* **1989**, *79*, 19. http://dx.doi.org/10.1016/0022-4596(89)90245-4.
(52) Inaba, H.; Nakashima, S.; Naito, K. Heat capacity of iron-chromium spinels, Fe3−xCrxO4. *Journal of Solid State Chemistry.* **1982**, *41*, 213. http://dx.doi.org/10.1016/0022-4596(82)90204-3.
(53) Szytuła, A.; Burewicz, A.; Dimitrijević, Ž.; Kraśnicki, S.; Rżany, H.; Todorović, J.; Wanic, A.; Wolski, W. Neutron Diffraction Studies of α-FeOOH. *physica status solidi (b).* **1968**, *26*, 429. 10.1002/pssb.19680260205.
(54) Wechsler, B. A.; Lindsley, D. H.; Prewitt, C. T. Crystal structure and cation distribution in titanomagnetites ($Fe_{3-x}Ti_xO_4$). *American Mineralogist.* **1984**, *69*, 754.

(55) Lukens, W. W.; Bucher, J. J.; Edelstein, N. M.; Shuh, D. K. Products of pertechnetate radiolysis in highly alkaline solution: Structure of $TcO_2 \cdot xH_2O$. *Environmental Science & Technology.* **2002**, *36*, 1124. 10.1021/es015653+.
(56) Downward, L.; Booth, C. H.; Lukens, W. W.; Bridges, F. In *13th International Conference on X-ray Absorption Fine Structure*; American Institute of Physics (AIP): Stanford, CA, USA, 2006, p 129. 10.1021/ic102111t.